Jour. Petrol. Soc. Korea
Vol. 3, No. 3, p. 220~233, 1994

Petrography and mineral chemistry of the granitic rocks in the Poeun-Sogrisan Area, Korea

Won Sik Cho*, Yong-Joo Jwa, Jong Ik Lee*** and Min Sung Lee***

**Department of Earth Science, Seoul National University, Seoul, 151-742, Korea.*
***Department of Geology, Gyeongsang National University, Chinju, 660-701, Korea.*
****Polar Research Center, Korea Ocean Research and Development Institute, Ansan P. O. Box 29, 425-600, Korea.*

ABSTRACT : The granitic rocks in the Poeun - Sogrisan area are composed of the Jurassic Poeun granodiorite and the Cretaceous Sogrisan granites. The latter can be divided into three rock types : coarse-grained biotite granite, porphyritic biotite granite and granite porphyry. Petrographical observations, especially focusing on the quartz-feldspar intergrowth texture, suggest that the Sogrisan granites has emplaced at shallower level and crystallized more rapidly than the Poeun granodiorite. The F, Cl contents and the Fe/(Fe+Mg) ratios of biotite and muscovite in the Sogrisan granites are higher than those in the Poeun granodiorite. The anorthite contents of plagioclase in the Poeun granodiorite are higher than in the Sogrisan granites. Ilmenite in the Sogrisan granites is more enriched in Mn and depleted in Fe than that in the Poeun granodiorite. The whole-rock magnetic susceptibility values (in 10^{-6} emu/g unit) are higher in the Sogrisan granites (33~144) than the Poeun granodiorite (9~12), indicating that the former generally belongs to magnetite-series granitoid and the latter to ilmenite-series one. The Sogrisan granites has solidified under more oxidizing environment than the Poeun granodiorite, judging from the whole-rock magnetic susceptibility measurements as well as the chemical compositions of biotite and ilmenite.

Key words : Poeun granodiorite, Sogrisan granites, petrography, mineral chemistry, whole-rock magnetic susceptibility

INTRODUCTION

In the central Ogcheon belt (the Poeun-Sogrisan area), Jurassic and Cretaceous granitic rocks are closely associated. Since 1970's many studies on these granitic rocks have been carried out (for example: Kim, 1971; Lee, 1971; Lee and Park, 1981; Shibata *et al.*, 1983; Kim and Shin, 1990; Yun and Kim, 1990; Jin *et al.*, 1992). However, petrographical and mineralogical differences between the Jurassic and Cretaceous granites in the belt are hardly known. It is necessary to determine these differences prior to invesitigating the genetical relationship between the two granitic masses of different age.

The purposes of this study are to describe the occurrence, petrography and mineral chemistry of the Jurassic Poeun granodiorite and the Cretaceous Sogrisan granitic rocks, and to examine their emplacement conditions and crystallization processes.

OUTLINE OF GEOLOGY

In the study area early Paleozoic metasedimentary rocks (so called "Ogcheon Supergroup") and Mesozoic granitic rocks are mainly cropped out (Fig. 1). Mesozoic granitic rocks can be divided into Jurassic granites (166 Ma) and Cretaceous ones (74~82 Ma) judging from their K-Ar biotite ages (Kim, 1971).

Paleozoic strata is mainly composed of phyllite, schist, amphibolite and limestone. They had suffered regional metamorphism of greenschist facies (Kim, 1971), and had been strongly deformed in middle to late Paleozoic (Cluzel *et al.*, 1990)

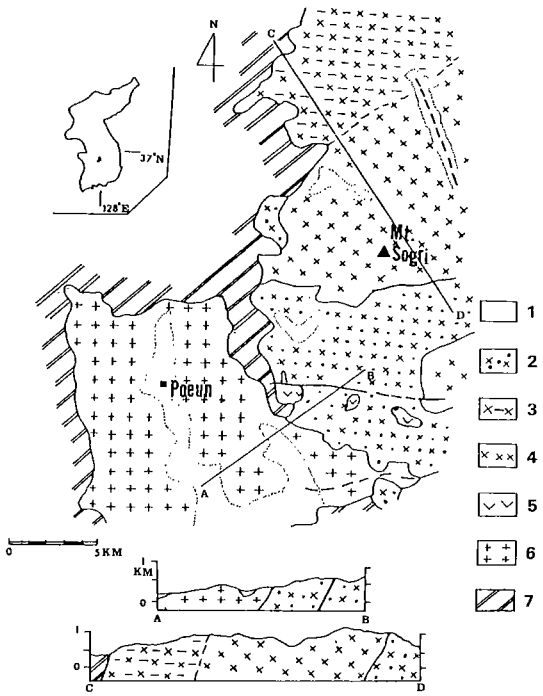

Fig. 1. Geologic map of the Poeun - Mt. Sogri area. 1; Alluvium, 2; Cretaceous granite porphyry (KGPH), 3; Cretaceous porphyritic biotite granite (KPGR), 4; Cretaceous coarse-grained biotite granite (KBGR), 5; Volcanic rocks, 6; Jurassic Poeun biotite granodiorite (JPGD), 7; Paleozoic Ogcheon Supergroup

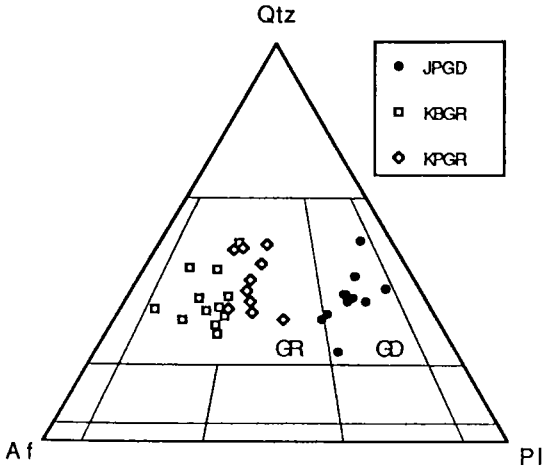

Fig. 2. Triangular diagram of modal compositions for the granitic rocks based on IUGS classification. Abbreviations : GR, Granite; GD, Granodiorite; Qtz, quartz; Af, alkali feldspar; Pl, plagioclase; JPGD, KBGR and KPGR are the same as those in Fig. 1.

Table 1. Average modal compositions of the granitic rocks

	JPGD	KBGR	KPGR
	12*	12*	15*
Qtz	31.2	34.7	37.8
Af	14.9	45.6	35.8
Pl	42.6	17.1	22.3
Bt	9.6	1.6	2.9
Mus	0.5	0.1	0.2
Zr	tr	0.1	0.1
Ap	0.2	0.1	0.1
Sph	0.3	-	-
Opq	0.1	0.3	0.4
All	tr	-	tr
Chl	0.2	0.1	0.1
C.I.	10.9	2.3	3.8

Abbreviations : Qtz=quartz; Af=alkali feldspar; Pl=plagioclase; Bt=biotite; Mus=muscovite; Zr=zircon; Ap=apatite; Sph=sphene; Opq=opaque minerals; All=allanite; Chl=chlorite; C.I.=color index; *=number of analyses.

or early Mesozoic time (Otoh *et al.*, 1990). The Jurassic Poeun granitic rocks (hereafter JPGD) occur as batholith in the southwestern part of the study area. They show granodioritic compositions in mode (Table 1, Fig. 2). Pyroxene- to amphibole-hornfelses in the metasediments develop around the JPGD (Lee and Park, 1981). In the western margin of the JPGD mass, the granitic rocks were slightly deformed. Muscovite-bearing, fine-grained felsic dikes several tens of centimeters in width intruded the JPGD with random directions.

Cretaceous granitic rocks (so called "Sogrisan Granites", hereafter KSGR) are texturally divided into coarse-grained biotite granite (KBGR), porphyritic biotite granite (KPGR) and granite porphyry (KGPH). The KBGR and the KPGR show granitic compositions in mode (Table 1, Fig. 2). The KPGR gradually changes to the KBGR in the northern part of Mt. Sogri (Sogrisan). The KBGR and some of the KPGR have miarolitic cavities or pegmatitic pockets, ranging from 1 cm to 30 cm in length. Euhedral quartz, alkali feldspar and rarely calcite have grown in the cavities. The amount of cavities increases toward the southern part of the KBGR. A number of pegmatitic and

aplitic dikes intruded into the KBGR and the KPGR. The KGPH, intruding the JPGD and the KBGR, is divided into three types by their phenocryst assemblages and color: pale gray granite porphyry, pinkish quartz feldspar porphyry and dark gray felsite. They show random distributions. The strata of volcanic tuff of andesitic to dacitic compositions are observed within the KGPH mass. The tuffaceous rocks are either lithic or crystalline. Purple lithic tuff contains subangular andesitic and dacitic fragments (0.5 cm to 10 cm in length). Black crystalline tuff has quartz, alkali feldspar and opaque minerals, showing flow structure. It is likely that the volcanic tuff has erupted before the intrusion of the KGPH since they contain no granitic rock fragments.

DESCRIPTION OF THE GRANITIC ROCKS

Jurassic Poeun Granodiorite (JPGD)

The JPGD is medium-grained equigranular granodiorite, and is mainly composed of plagioclase, quartz, alkali feldspar and biotite. Sphene, apatite, zircon, allanite and ilmenite are also observed as accessory minerals. Secondary minerals are muscovite and chlorite. Plagioclase is euhedral to subhedral and shows strong compositonal zonation of andesine to oligoclase. It has sericitized core and sometimes exhibits oscillatory zoning. Biotite, apatite, opaque minerals and early crystallized plagioclase are observed within plagioclase grains as inclusions. Subhedral quartz forms an aggregate of several grains, showing slightly undulatory extinction. It contains biotite and rarely sphene. Alkali feldspar is mainly microcline and contains inclusions of plagioclase, quartz, biotite, sphene and early microcline. In the deformed rocks, myrmekites occur along the marginal parts of microcline. Dark brown anhedral biotite fills the interstice, and shows linear arrangement in the deformed rocks. Large euhedral sphene contains a number of anhedral ilmenite grains like Jurassic Andong granodiorite (Lee and Lee, 1991). Muscovite-bearing, fine-grained felsic dike (JMFD) is composed of quartz, microcline and muscovite with subordinate amounts of plagioclase and biotite. Judging from the whole-rock chemistry, the JMFD is considered to be *in situ* fractionation product of the JPGD (Jwa *et al.*, in prep.).

Cretaceous Coarse-grained Biotite Granite (KBGR)

Pinkish KBGR is mainly composed of quartz, alkali feldspar, plagioclase and biotite. Accessory minerals are apatite, zircon, allanite, magnetite and ilmenite. Chlorite and muscovite are secondary minerals. Subhedral to anhedral quartz exhibits undulatory extinction. Some of large quartz grains contain biotite and rarely secondary muscovite along their fractures. Embayed quartz grains are usually intergrown with alkali feldspar. Alkali feldspar occurs as anhedral perthitic orthoclase filling the interstices. Large grains show the Carlsbad twinning and contain plagioclase, biotite and anhedral quartz as inclusions. Subhedral plagioclase is oligoclase in compositon and forms an aggregate of several grains. Greenish brown biotite contains apatite and zircon, and is partly altered to chlorite and muscovite. Accessory allanite and magnetite accompanied by ilmenite are associated with biotite.

Cretaceous Porphyritic Biotite Granite (KPGR)

The KPGR is leucocratic fine- to medium-grained porphyritic biotite granite and consists of quartz, alkali feldspar, plagioclase and biotite. Apatite, zircon, allanite, magnetite and ilmenite are accessory minerals. Phenocrysts are euhedral quartz (up to 10 mm) and perthitic orthoclase (up to 15 mm). Quartz phenocrysts show slightly undulatory extinction, and rarely contains secondary muscovite. Perthitic orthoclase phenocrysts usually contain plagioclase, biotite and anhedral quartz.

Table 2. Chemical compositions and structural formulae of biotites

sample	KPGR				KBGR		JPGD							
	K0101	K0104	K1406	K1408	K1504	K1606	J0209A	J1715	J1716	J1718	J1719A	J1720	J0713	J0715
SiO_2	36.03	36.18	35.64	35.72	35.10	34.94	35.18	35.96	36.96	36.12	36.46	35.86	35.27	35.46
Al_2O_3	14.37	12.72	14.01	14.52	13.02	12.78	18.44	15.99	15.68	15.26	15.34	15.92	17.33	17.05
TiO_2	3.41	3.30	3.37	3.12	3.37	2.42	3.02	3.28	2.42	3.05	3.35	3.36	3.21	3.46
FeO*	27.83	28.43	28.82	27.59	31.63	33.41	23.27	24.25	23.74	24.12	23.10	24.35	23.61	24.01
MnO	1.91	1.00	1.97	1.83	0.73	0.86	0.47	0.42	0.36	0.36	0.35	0.35	0.62	0.56
MgO	3.08	5.40	3.30	3.50	3.74	3.04	6.40	6.75	7.86	7.91	8.00	7.11	6.55	6.64
CaO	0.00	0.07	0.00	0.00	0.04	0.05	0.00	0.01	0.00	0.02	0.00	0.01	0.00	0.00
Na_2O	0.09	0.09	0.15	0.12	0.19	0.16	0.08	0.06	0.04	0.05	0.05	0.06	0.05	0.07
K_2O	9.23	9.06	9.02	9.14	8.86	8.31	9.52	9.46	9.57	9.52	9.60	9.68	9.74	9.69
Cl	0.15	0.19	0.16	0.14	0.32	0.27	0.02	0.01	0.02	0.01	0.02	0.02	0.04	0.04
=O	−0.03	−0.04	−0.04	−0.03	−0.07	−0.06	−0.01	−0.00	−0.01	−0.00	0.00	0.00	−0.01	−0.01
F	1.96	1.03	2.06	1.68	1.52	0.90	0.24	0.65	0.69	0.41	0.39	0.54	0.27	0.34
=O	−0.83	−0.43	−0.87	−0.52	−0.64	−0.38	−0.10	−0.27	−0.29	−0.17	−0.17	−0.22	−0.11	−0.15
Total	97.20	97.00	97.59	96.81	97.81	96.70	96.53	96.29	96.94	96.66	96.49	97.04	96.57	97.16
Recalculated on 22 oxygens														
Si	5.7402	5.7489	5.6895	5.7090	5.6405	5.6979	5.4045	5.5710	5.6629	5.5830	5.6135	5.5382	5.4498	5.4472
Al IV	2.2598	2.2511	2.3105	2.2910	2.3595	2.3021	2.5955	2.4290	2.3371	2.4170	2.3865	2.4618	2.5502	2.5528
VI	0.4390	0.1319	0.3293	0.4438	0.1054	0.1548	0.7431	0.4907	0.5020	0.3635	0.3970	0.4354	0.6052	0.5459
Ti	0.4090	0.3948	0.4046	0.3751	0.4065	0.2964	0.3485	0.3825	0.2801	0.3549	0.3871	0.3903	0.3733	0.3991
Fe	3.7075	3.7785	3.8480	3.6880	4.2507	4.5564	2.9902	3.1423	3.0505	3.1191	2.9749	3.1452	3.0507	3.0847
Mn	0.2578	0.1342	0.2661	0.2474	0.0994	0.1193	0.0617	0.0555	0.0469	0.0465	0.0450	0.0463	0.0806	0.0722
Mg	0.7322	1.2787	0.7858	0.8347	0.8969	0.7397	1.4655	1.5589	1.7995	1.8232	1.8365	1.6360	1.5091	1.5208
Ca	0.0000	0.0117	0.0006	0.0000	0.0070	0.0092	0.0002	0.0017	0.0006	0.0028	0.0019	0.0019	0.0000	0.0003
Na	0.0267	0.0275	0.0448	0.0335	0.0602	0.0496	0.0247	0.0168	0.0119	0.0155	0.0158	0.0176	0.0157	0.0208
K	1.8762	1.8370	1.8362	1,8637	1.8168	1.7286	1.8664	1.8698	1.8749	1.8774	1.8847	1.9062	1.9190	1.8986
Cl	0.0392	0.0524	0.0438	0.0370	0.0869	0.0761	0.0056	0.0020	0.0059	0.0059	0.0049	0.0043	0.0091	0.0090
F	0.9867	0.5168	1.0417	0.8480	0.7729	0.4658	0.1175	0.3191	0.3357	0.2013	0.1924	0.2650	0.1300	0.1724
OH	2.9741	3.4308	2.5203	3.1150	3.1402	3.4581	3.8769	3.6789	3.6584	3.7928	3.8027	3.7307	3.8609	3.8186
Fe/Fe+Mg	0.8351	0.7472	0.8304	0.8154	0.8258	0.8603	0.6711	0.6684	0.6290	0.6311	0.6183	0.6578	0.6690	0.6698
F/(F+OH)	0.2491	0.1309	0.2140	0.2140	0.1975	0.1187	0.0294	0.0798	0.0840	0.0504	0.0482	0.0663	0.0326	0.0432

*; total Fe as FeO

Smaller grains in the groundmass are composed of anhedral quartz, orthoclase, plagioclase and biotite. Micrographic intergrowths of quartz and alkali feldspar are frequently developed in the groundmass. Subhedral plagioclase is oligoclase and has sericitized cores. Dark brown biotite with serriate grain boundaries (up to 5 mm) contains apatite, zircon and opaque minerals. Magnetite is intimately associated with ilmenite.

Cretaceous Granite Porphyry (KGPH)

Phenocrysts of pale gray granite porphyry (30-40% in volume percentage) are orthoclase, plagioclase, quartz and biotite in order of abundance. Euhedral orthoclase (up to 7 mm, about 40% in phenocrysts) shows the Carlsbad twinning, and contains plagioclase and anhedral quartz. Subhedral plagioclase is strongly sericitized. Anhedral quartz (up to 3 mm, about 30%) shows embayed grain boundaries. Anhedral, red to dark brown biotite oxidized at subsolidus condition is associated with opaque minerals. Groundmass is composed of anhedral quartz, orthoclase, plagioclase and biotite. Pale green anhedral hornblende is

rarely observed.

Pinkish quartz feldspar porphyry has many small cavities (up to 2 mm). Subhedral quartz phenocryst has sharp and/or locally embayed grain boundaries. Large euhedral orthoclase (up to 9 mm) displays the Carlsbad twinning, and contains occasionally anhedral quartz and plagioclase. Anhedral biotite, plagioclase and opaque minerals occur as minor constituents. Groundmass is cryptocrystalline and/or microcrystalline and shows micrographic and spherulitic textures.

Dark gray felsite is mainly composed of small anhedral quartz and spherulite. Secondary calcite, chloritized biotite and opaque minerals are rarely observed.

MINERALOGY

The chemical compositions of biotite, plagioclase, alkali feldspar, ilmenite and muscovite in the granitic rocks were analyzed by an electron microprobe analyzer (JXA-733 Mark II, JEOL) of the Geological Institute, Universty of Tokyo, following the procedure described by Nakamura and Kushiro (1970). Acceleration voltage and beam current conditions except for the analysis of ilmenite were 15 kV and 1.2×10^{-8} A, respectively. Ilmenite was analyzed at 20 kV of acceleration voltage.

Biotite

Subhedral to anhedral biotite usually contains apatite, zircon and opaque minerals. It partly alters to chlorite and muscovite. Some grains in the KBGR suffered secondary oxidation caused by the breakdown to Fe-Ti oxides, quartz and alkali feldspar. In the KPGR, biotite sometimes occurs as large grains (5 to 8 mm).

Table 2 lists the chemical compositions of biotite. The Mg/(Mg+Fe) ratios of biotite in the JPGD are generally higher than 0.3, and those in the KSGR (the KPGR and the KBGR) is lower than 0.3. Total Al contents of biotite in the JPGD

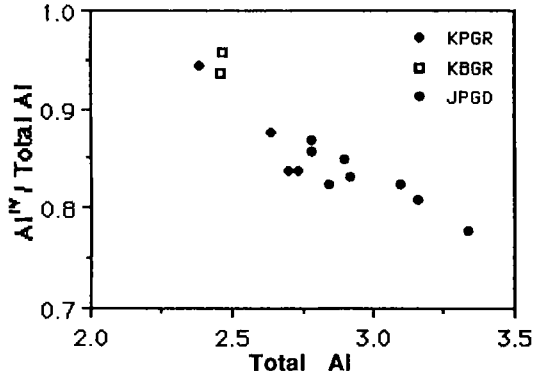

Fig. 3. Al^{IV}/Total Al plotted against Total Al of biotities.

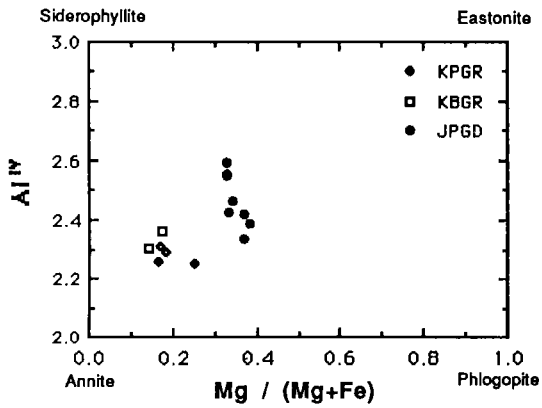

Fig. 4. Al^{IV} plotted against Mg/(Mg+Fe) of biotites.

range from 2.7 to 3.4, whereas those in the KSGR is lower than 2.7. As shown in Fig. 3, the ratios of tetrahedral Al (Al^{IV}) to total Al contents decrease with the increase of total Al contents, indicating the increase of the ratios of octahedral Al (Al^{VI}). Biotite of the JPGD shows more variation in Al^{IV} contents than that of KSGR (Fig. 4). Concerning the substitutions of elementes between octahedral and tetrahedral sites, biotite of the JPGD seems to have been substituted as follows : $Ti^{VI}+2Al^{IV}=Mg^{VI}+2Si^{IV}$. But elemental substitution in biotite of the KSGR is not clear (Fig. 5).

The fluorine contents of the KSGR range from 0.4 to 1.0, whereas those of the JPGD are lower than 0.3. Biotite of the JPGD is almost chlorine-free. The relative ratios of F, Cl and OH in hydroxyl sites are shown in Fig. 6. Hydroxyl ion

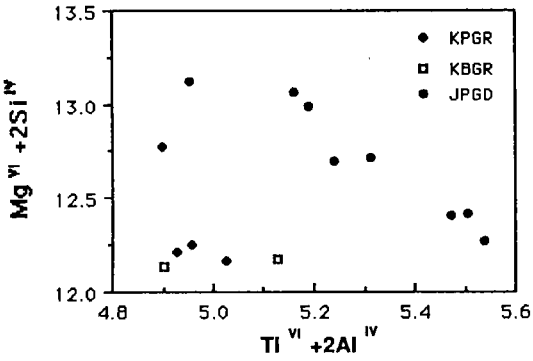

Fig. 5. ($Mg^{VI}+2Si^{IV}$) plotted against ($Ti^{VI}+2Al^{IV}$) of biotites.

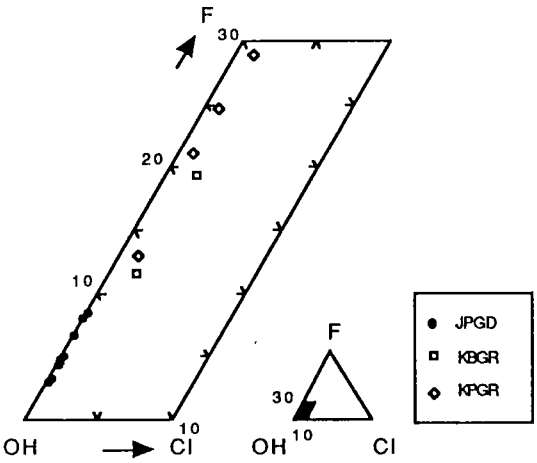

Fig. 6. Triangular diagram of F-OH-Cl contents in hydroxyl sites of biotites.

(OH) in biotite of the KSGR is more replaced by F and Cl than that of the JPGD. Fluorine enrichment in biotite of the KSGR corroborates the experimental result that fluorine is concentrated in granitic melts relative to aqueous fluids (Webster and Holloway, 1990).

Plagioclase

Plagioclase of the JPGD is strongly zoned, and has sericitized cores. Some grains exhibit oscillatory zonings. Albite twinned plagioclase of the KSGR is partly sericitized, and forms an aggregate of several grains. Chemical compositions and structural formulae of plagioclase are listed in

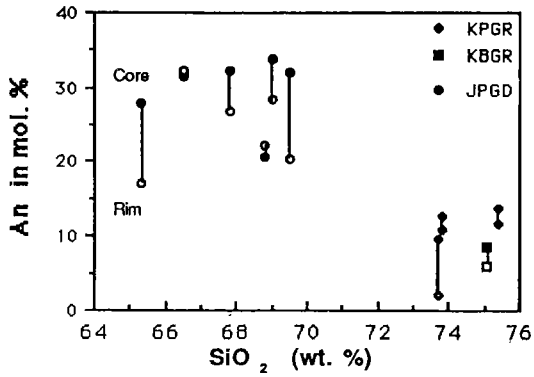

Fig. 7. The An contents (mol.%) of plagioclases plotted against SiO_2 (wt.%) of the host granitic rocks.

Table 3. The anorthite (An) contents of plagioclase in the JPGD are greater than those in the KSGR. Most of them are normally zoned, but some grains reversely zoned. The differneces of An contents between core and rim in the JPGD are generally larger than in the KSGR (Fig. 7). Therefore, the granitic magma of the JPGD seems to have had longer duration in plagioclase primary field defined by Tuttle and Bowen (1958) than that of the KSGR, regardless of pressure difference between two granitic masses.

Alkali Feldspar

Alkali feldspar is microcline in the JPGD and perthitic orthoclase in the KSGR. Microcline in the JPGD has crystallized later than any other constituents including plagioclase, biotite and quartz. Perthitic orthoclase in the KPGR usually occurs as large phenocryst. String and patch type albite exsolutions are predominant. Anhedral alkali feldspar in the KSGR is intergrown with quartz. It is thus expected that the liquidus of alkali feldspar in the KSGR was higher than that of plagioclase, while this state was reverse in the JPGD. The chemical compositions of alkali feldspar are shown in Table 4. The geothermometer of coexisting plagioclase and alkali feldspar determined by Powell and Powell (1977) yield that the temperature of KSGR was 350℃ to 490℃, and

Table 3. Chemical compositions of plagioclases

Rock	KSGR								JPGD														JMFD			
	K1406		K1408		K0101		K1606		J0209A		J1715		J1716		J1718		J1719A		J1720		J0713		J0209B		J0716B	
	core	rim	core	rim	core	rim	core	rim	core	rim	core	rim	core	rim	core	rim	core	rim	core	rim	core	rim	core	rim	core	rim
SiO_2	65.90	64.67	65.28	65.74	67.02	68.75	66.66	67.27	60.65	62.01	59.60	61.57	61.69	64.67	60.42	60.25	58.69	61.53	62.12	63.33	59.18	63.31	67.42	67.66	68.41	69.28
Al_2O_3	20.78	21.34	21.29	21.18	20.33	19.33	20.17	19.71	24.70	23.82	25.03	24.21	23.95	22.02	24.33	24.77	25.67	23.99	23.66	23.12	24.69	22.56	20.40	20.17	19.61	19.41
TiO_2	0.01	0	0.05	0.04	0.04	0.02	0.01	0.00	0.01	0.04	0.02	0.00	0.02	0.01	0.01	0.02	0.03	0.00	0.00	0.02	0.03	0.02	0.02	0.01	0.00	0.00
FeO*	0.14	0.14	0.11	0.06	0.13	0.04	0.13	0.09	0.03	0.06	0.01	0.05	0.04	0.12	0.00	0.02	0.11	0.08	0.11	0.05	1.34	0.02	0.01	0.01	0.04	0.02
MnO	0.03	0.03	0.02	0.01	0.01	0.01	0.00	0.02	0.04	0.03	0.00	0.00	0.00	0.01	0.00	0.00	0.05	0.02	0.01	0.02	0.05	0.02	0.00	0.03	0.03	0.02
MgO	0.01	0	0.02	0	0.01	0.01	0.00	0.01	0.00	0.01	0.01	0.01	0.02	0.01	0.00	0.00	0.00	0.00	0.01	0.00	0.08	0.01	0.01	0.01	0.01	0.00
CaO	2.29	2.63	2.86	2.44	1.93	0.41	1.74	1.24	6.74	5.60	7.12	5.91	5.73	3.52	6.44	6.66	7.75	5.80	5.56	4.63	6.46	4.23	1.69	1.32	0.35	0.46
Na_2O	10.16	9.77	9.65	9.80	9.62	10.93	9.56	9.91	7.69	8.31	7.52	8.22	8.13	9.38	7.49	7.64	7.25	8.20	8.22	8.79	7.23	9.06	10.35	10.81	11.29	11.28
N_2O	0.46	0.4	0.52	0.35	0.75	0.16	1.10	1.23	0.15	0.23	0.22	0.12	0.13	0.19	0.34	0.16	0.13	0.19	0.17	0.20	0.50	0.20	0.10	0.12	0.14	0.11
Total	99.78	100.07	99.70	99.66	99.84	99.66	99.37	99.48	100.01	100.11	99.53	100.09	99.71	99.93	99.03	99.52	99.68	99.81	99.86	100.16	99.56	99.41	100.00	100.14	99.88	100.49
Recalculated on 8 oxygens																										
Ca	0.108	0.124	0.136	0.115	0.091	0.019	0.083	0.059	0.321	0.266	0.342	0.282	0.273	0.166	0.310	0.319	0.372	0.276	0.187	0.219	0.312	0.202	0.079	0.062	0.016	0.201
Na	0.869	0.832	0.827	0.838	0.819	0.927	0.820	0.848	0.663	0.714	0.653	0.706	0.701	0.802	0.652	0.661	0.630	0.707	0.708	0.753	0.631	0.780	0.878	0.916	0.957	0.941
K	0.026	0.022	0.029	0.020	0.042	0.009	0.062	0.070	0.009	0.013	0.012	0.007	0.007	0.010	0.020	0.009	0.007	0.011	0.009	0.011	0.029	0.011	0.006	0.007	0.008	0.006
An	10.8	12.6	13.7	11.8	9.6	2.0	8.6	6.0	32.3	26.8	33.9	28.3	27.8	17.0	31.6	32.2	36.9	27.8	20.7	22.3	32.1	20.3	8.2	6.3	1.7	2.2
Ab	86.6	84.8	83.3	86.1	86.0	97.1	85.0	86.9	66.8	71.9	64.9	71.0	71.5	81.9	66.4	66.9	62.4	71.1	78.3	76.6	64.9	78.6	91.2	93.0	97.5	97.2
Or	2.6	2.6	3.0	2.1	4.4	0.9	6.4	7.1	0.9	1.3	1.2	0.7	0.7	1.1	2.0	0.9	0.7	1.11	1.0	1.1	3.0	1.1	0.6	0.7	0.8	0.6

*; total Fe as FeO

Table 4. Chemical compositions of alkali feldspars

a) Perthitic orthoclases in the Cretaceous Sogrisan granites

Rock	KPGR								KBGR			
	K0101		K0104		K1406		K1408		K1606		K1613	
	af	pl	af	pl	af	pl	af	pl	af	pl	af	pl
SiO_2	65.20	69.04	66.27	68.23	64.92	68.21	66.23	67.85	64.62	69.13	65.18	68.25
Al_2O_3	18.01	18.77	17.97	19.67	18.10	19.40	18.38	19.90	17.72	19.00	18.11	19.34
TiO_2	0.01	0.00	0.05	0.03	0.01	0.00	0.04	0.00	0.02	0.00	0.06	0.02
FeO*	0.06	0.04	0.03	0.03	0.08	0.05	0.05	0.04	0.00	0.04	0.03	0.00
MnO	0.03	0.00	0.02	0.04	0.00	0.06	0.03	0.03	0.00	0.00	0.08	0.02
CaO	0.04	0.02	0.04	0.89	0.00	0.62	0.01	1.09	0.00	0.01	0.00	0.56
MgO	0.01	0.01	0.00	0.01	0.01	0.00	0.01	0.00	0.00	0.01	0.00	0.01
Na_2O	0.68	7.88	1.72	10.44	0.61	11.24	2.39	10.60	0.20	11.17	0.25	10.59
K_2O	15.42	4.91	13.72	0.29	15.52	0.30	12.8	0.24	16.43	0.10	16.28	0.60
Total	99.46	100.67	99.82	99.63	99.25	99.88	100.03	99.75	99.19	99.55	99.99	99.39
Recalculated on 8 oxygens												
Ca	0.0021	0.0010	0.0020	0.0417	0.0000	0.0293	0.0003	0.0509	0.0000	0.0045	0.0000	0.0263
Na	0.0610	0.6710	0.1501	0.8867	0.0545	0.9549	0.2114	0.9007	0.0185	0.9471	0.0224	0.9027
K	0.9102	0.2750	0.8030	0.0162	0.9182	0.0165	0.7486	0.0133	0.9760	0.0053	0.9595	0.0335
An	0.2	0.1	0.2	4.4	0.0	2.9	0.0	5.3	0.0	0.4	0.0	2.7
Ab	6.3	70.9	15.7	93.9	5.6	95.4	22.0	93.3	1.9	99.0	2.3	93.8
Or	93.5	29.0	84.1	1.7	94.4	1.7	78.0	1.4	98.1	0.6	97.7	3.5

*; total Fe as FeO

b) Microclines in Jurassic Poeun granodiorite

Rock	JPGD						JMFD	
	J0209A	J1715	J1716	J1719A	J1720	J0713	J0209B	J0716B
SiO_2	65.04	65.49	65.51	65.40	65.69	65.06	65.72	65.90
Al_2O_3	18.38	18.12	18.12	18.11	18.30	18.02	18.14	17.91
TiO_2	0.05	0.00	0.02	0.06	0.03	0.04	0.01	0.01
FeO*	0.02	0.02	0.06	0.03	0.00	0.06	0.03	0.01
MnO	0.02	0.02	0.00	0.01	0.03	0.01	0.02	0.01
CaO	0.00	0.00	0.01	0.02	0.06	0.01	0.00	0.03
Na_2O	0.79	0.86	0.83	1.05	1.58	0.96	0.48	0.57
K_2O	15.33	15.23	15.17	15.1	14.34	15.15	15.72	15.85
Total	99.63	99.73	99.73	99.78	100.03	99.31	100.34	100.35
Recalculated on 8 oxygens								
Ca	0.0000	0.0002	0.0005	0.0007	0.0030	0.0006	0.0000	0.0015
Na	0.0708	0.0769	0.0744	0.0936	0.1399	0.0858	0.0427	0.0503
K	0.0931	0.8952	0.8910	0.8871	0.8391	0.8968	0.9322	0.9278
An	0.0	0.0	0.1	0.1	0.3	0.1	0.0	0.2
Ab	7.3	7.9	7.7	9.5	14.2	8.7	4.4	5.1
Or	92.7	92.1	92.2	90.4	85.5	91.2	95.6	94.7

that of the JPGD was about 250℃ at 1 to 3 kbar. These results, however, cannot give any useful informations on the magmatic crystallization because their temperatures are considerably lower than those expected for solidus of granitic magma.

Table 5. Chemical compositions of ilmenites

Rock	JPGD					KPGR			
	J0209A	J1715	J1716	J1718	J1720	K0101	K0104	K1406	K1408
SiO_2	0.05	0.02	0.04	0.04	0.02	0.08	0.02	0.03	0.06
Al_2O_3	0.04	0.01	0.01	0.03	0.01	0.01	0.01	0.04	0.03
TiO_2	52.14	52.37	52.13	52.35	51.48	50.10	50.09	49.77	52.97
FeO*	37.79	41.97	44.44	42.41	45.13	29.78	38.58	32.84	35.56
MnO	9.16	5.18	2.79	4.20	3.13	16.85	9.59	11.71	7.14
MnO	0.04	0.02	0.05	0.01	0.01	0.01	0.00	0.01	0.01
CaO	0.02	0.01	0.22	0.16	0.02	0.02	0.05	0.00	0.01
Na_2O	0.00	0.00	0.00	0.01	0.00	0.00	0.01	0.00	0.01
Na_2O	0.05	0.01	0.01	0.01	0.01	0.01	0.01	0.03	0.00
V_2O_3	0.28	0.14	0.21	0.18	0.25	0.21	0.19	0.21	0.25
Cr_2O_3	0.01	0.01	0.03	0.00	0.01	0.00	0.03	0.00	0.02
Total	99.27	99.59	99.69	99.22	99.81	96.86	98.36	94.43	95.79
	Recalculated on 3 oxygens								
Si	0.0013	0.0006	0.0009	0.0010	0.0005	0.0020	0.0005	0.0007	0.0016
Ti	0.9930	0.9926	0.9877	0.9781	0.9602	0.9744	0.9621	0.9975	1.0489
Fe	0.8004	0.8846	0.9364	0.8811	0.9360	0.6441	0.8240	0.7319	0.7830
Mg	0.0014	0.0060	0.0017	0.0049	0.0059	0.0005	0.0000	0.0002	0.0004
Ca	0.0005	0.0003	0.0060	0.0421	0.0007	0.0050	0.0013	0.0000	0.0002
Mn	0.1966	0.1107	0.0596	0.0884	0.0657	0.3692	0.2074	0.2639	0.1592
Al	0.0011	0.0004	0.0030	0.0009	0.0002	0.0004	0.0003	0.0012	0.0009
V	0.0056	0.0029	0.0043	0.0036	0.0300	0.0044	0.0039	0.0045	0.0053
Cr	0.0002	0.0020	0.0005	0.0000	0.0009	0.0001	0.0005	0.0000	0.0004

*; total Fe as FeO

Ilmenite

Anhedral ilmenite in the JPGD occurs in euhedral sphene as inclusion, and that in the KSGR accompanies magnetite. The chemical compositions of ilmenite are shown in Table 5. Total Fe contents of ilmenite in the KPGR are lower, and Mn contents higher than those in the JPGD (Fig. 8).

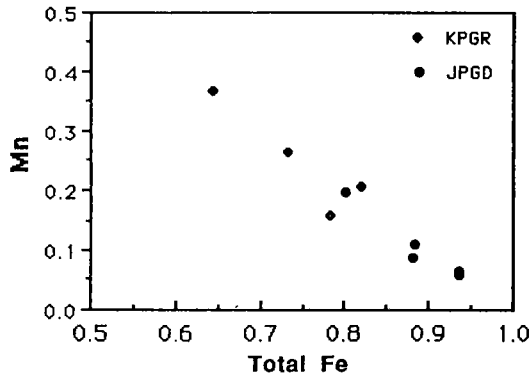

Fig. 8. Mn contents plotted against total Fe of ilmenite.

Muscovite

Muscovite is mainly observed in core of plagioclase in the JPGD, and anhedral muscovite (about 2.4 vol.%) in felsic dike (JMFD) shows interstitial feature. Anhedral muscovite in KSGR is observed in large quartz grains. Table 6 displays the chemical compositions and structural formulae of muscovite. The F/(F+OH) ratios of muscovite in the KSGR are higher and the Mg/(Mg+Fe) ratios are lower than those in the JPGD, which are similar to biotite compositions. It seems that muscovites have experienced the celadonite substitution, that is, octahedral Al is replaced by

Table 6. Chemical compositions and structural formulae of muscovites

Rock	KSGR			JPGD					JMFD	
	K1406	K1504	K1606	J0209A	J1716	J1718	J0713	J0715	J0209B	J0716B
SiO_2	47.88	47.78	47.57	49.40	49.00	49.46	49.44	49.83	47.32	48.55
Al_2O_3	34.05	32.43	36.64	32.00	37.03	32.33	32.59	31.54	34.45	30.81
TiO_2	0.06	0.25	0.01	0.45	0.00	0.10	0.02	0.35	0.39	0.47
FeO*	4.81	5.57	0.83	2.94	0.09	2.62	3.05	3.79	2.81	5.36
MnO	0.20	0.20	0.14	0.05	0.00	0.00	0.06	0.02	0.03	0.02
MgO	0.41	0.41	0.01	1.30	0.08	1.74	0.95	1.54	0.47	1.01
CaO	0.00	0.00	0.01	0.01	0.03	0.02	0.00	0.00	0.01	0.01
Na_2O	0.19	0.45	0.60	0.21	0.12	0.14	0.21	0.22	0.40	0.18
K_2O	7.83	8.57	9.62	9.70	9.56	10.20	10.06	9.18	9.66	9.71
Cl	0.00	0.01	0.00		0.01	0.00	0.00	0.01		0.01
=O	0.00	0.00	0.00		0.00	0.00	0.00	0.00		0.00
F	0.96	1.52	1.19		0.08	0.09	0.14	0.13		0.33
=O	−0.40	−0.64	−0.50		−0.03	−0.04	−0.06	−0.06		−0.14
Total	95.99	96.55	96.12	96.06	95.97	96.66	96.46	96.55	95.54	96.32
Recalculated on 22 oxygens										
Si	6.2821	6.3202	6.2373	6.4695	6.3390	6.4582	6.4704	6.4993	6.2470	6.4229
Al IV	1.7179	1.6798	1.7627	1.5305	1.6610	1.5418	1.5296	1.5007	1.7530	1.5771
VI	3.5481	3.3773	3.8997	3.4296	3.9847	3.4315	3.4965	3.3486	3.6078	3.2270
Ti	0.0054	0.0248	0.0007	0.0439	0.0003	0.0097	0.0019	0.0345	0.0387	0.0467
Fe	0.4752	0.5554	0.0816	0.2899	0.0082	0.2579	0.3003	0.3725	0.2791	0.5332
Mn	0.0226	0.0219	0.0159	0.0055	0.0000	0.0000	0.0063	0.0025	0.0030	0.0026
Mg	0.0798	0.0815	0.0011	0.2529	0.0150	0.3391	0.1853	0.2984	0.0925	0.1997
Ca	0.0003	0.0000	0.0007	0.0020	0.0036	0.0023	0.0006	0.0040	0.0014	0.0018
Na	0.0940	0.1146	0.1512	0.0528	0.0311	0.0348	0.0529	0.0549	0.1027	0.0452
K	1.3113	1.4464	1.6092	1.6210	1.5778	1.6992	1.6797	1.5269	1.6275	1.6390
Cl	0.0008	0.0014	0.0000		0.0013	0.0000	0.0004	0.0017		0.0019
F	0.3985	0.6370	0.4947		0.0330	0.0359	0.0575	0.0055		0.1385
OH	3.6007	3.3616	3.5053		3.9657	3.9641	3.9421	3.9928		3.8596

*; total Fe as FeO

Mg and Fe, and tetrahedral Al by Si (Fig. 9). The substitutional correlation among these elements can be deduced as follows (from Konings *et al.*, 1988):

$$Al^{IV}+R^{3+}=Si+R^{2+}\ (R^{3+}=Al^{VI},\ Fe;\ R^{2+}=Mg^{2+},\ Mn^{2+}).$$

From the TiO_2-FeO* (total Fe)-MgO triangular diagram (Fig. 10), muscovites of the granitic rocks in the study area generally have low TiO_2 contents, but those of KSGR have relatively high FeO* contents. Compared with the chemical compositions of muscovites in leucocratic granite of Millevaches massif studied by Monier *et al.* (1984), muscovites in the study area have been formed by secondary alteration at subsolidus state.

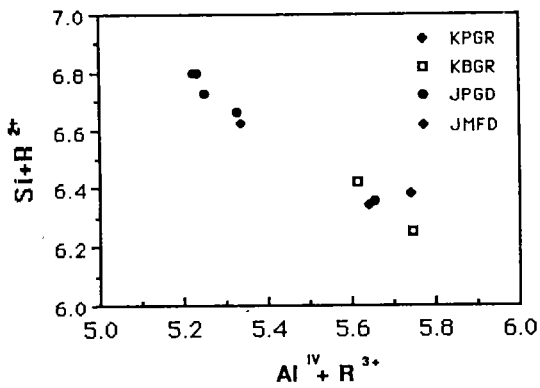

Fig. 9. $(Si+R^{2+})$ plotted against $(Al^{IV}+R^{3+})$ of muscovites.

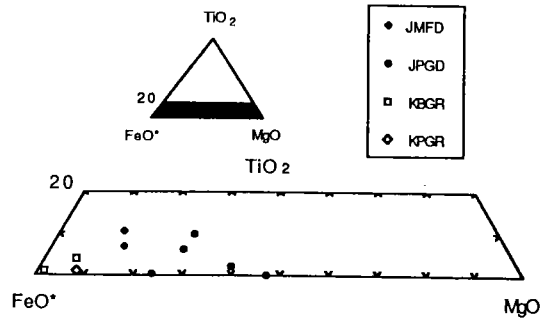

Fig. 10. Triangular diagram of TiO_2-FeO* (total Fe)-MgO contents of muscovites.

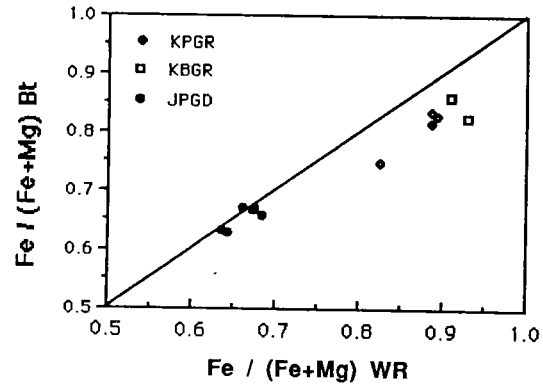

Fig. 11. Fe/(Mg+Fe) of biotites plotted against Fe/(Mg+Fe) of the host granitic rocks.

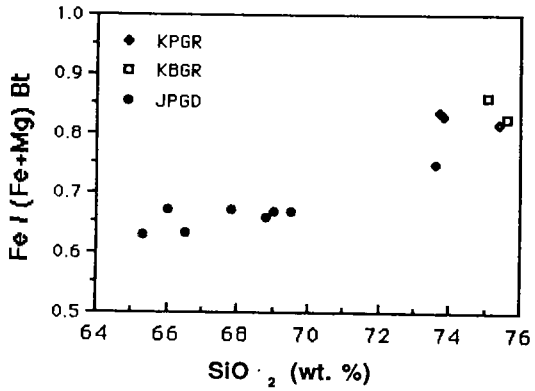

Fig. 12. Fe/(Mg+Fe) of biotites plotted against SiO_2 (wt.%) of the host granitic rocks.

DISCUSSION

The characteristic quartz-feldspar intergrowth texture in the granitic rocks in the study area appears in two modes: myrmekitic in the JPGD and micrographic in the KSGR. In the Mesozoic granitic rocks in Korea, the myrmekitic texture appears in the Jurassic granites and the micrographic texture in the Cretaceous ones (for example, Iiyama and Fonteilles, 1981). The petrographical observations for the granitic rocks in the study area corroborates the previous reports. The different quartz-feldspar intergrowth in the Mesozoic granites in Korea indicates the different emplacement condition in two granitic bodies of different age. Generally the Jurassic granitic pluton emplaced deeper part of the crust than the Cretaceous one (Cho and Kwon, 1994). Thus the different intergrowth texture is likely to be controlled by the depth, more precisely by the decompressing and cooling path at the level the magma has emplaced.

In the Cretaceous granitic rocks, the micrographic texture represents the simultaneous crystallization of quartz and alkali feldspar under the undercooling with isothermal decompression (Lee, 1991). The exsolution or degassing of vapour phases, evidenced from the existence of miarolitic cavity or pegmatitic pocket, increases the degree of undercooling. In addition, the spherulitic texture of quartz-feldspar intergrowth sometimes occurs in the KSGR. This texture is generally formed by the rapid crystallization from the viscous granitic magma. These petrographic results suggest that the KSGR has rapidly solidified at the shallower level. The myrmekitic texture can be formed in three ways : (1) from the volume for volume replacement of the marginal parts of alkali feldspar in contact with plagioclase (Shelly, 1964), (2) from the micropressure quenching during the separation of an aqueous phase as crystallization progresses (Hibbard, 1979), and (3) from the subsitution for alkali feldspar induced by deformation at subsolidus state (Simpson and Wintsch, 1989). The replacement with co-precipitation of quartz cannot wholly be explained by exsolution from the host alkali feldspar, as it requires a net gain of sodium and calcium with a loss of pota-

ssium from the system. The latter two ways need local tectonic events such as deformation for the formation of the intergrowth. In the JPGD, the myrmekitic texture is easily observed along the marginal part of microcline in the deformed samples. Though we have no evidence whether the role of the deformation is direct or indirect, it seems like that the deformation has more or less affected the formation of the intergrowth. Nevertheless the origin of the texture is still uncertain and more studies are needed. Alkali feldspar is microcline in the JPGD and perthitic orthoclase in the KSGR. Since microcline is more stable phase at the lower temperature field than the perthitic orthoclase, the occurrence of microcline in the JPGD may indicate that the JPGD has more slowly solidified at the deeper level than the KSGR.

Compared with whole-rock chemistry (Jwa *et al.*, in prep.), the Fe/(Fe+Mg) ratios in biotite of the KSGR are lower than those of whole-rock, and those of the JPGD are nearly the same as those of whole-rock (Fig. 11). This discrepancy of Fe/(Fe+Mg) ratios between mineral and whole-rock in the KSGR would have been caused by fractional crystallization of mafic minerals including magnetite (Tsusue *et al.*, 1984). Thus it seems likely that the KSGR has been crystallized under more oxidizing conditions than the JPGD. Furthermore, the Fe/(Fe+Mg) ratios of biotite in the JPGD slightly increase with the increase of whole-rock SiO_2 contents, whereas those in the KSGR are dispersed (Fig. 12). This is due to the crystallization of biotite in the JPGD under buffered condition of oxygen fugacity (Wones and Eugster, 1965; Czamanske *et al.*, 1981).

The compositional differences of ilmenite are caused by the condition of crystallization, especially by the oxygen fugacity. Ilmenite in the KPGR has lower total Fe contents and higher Mn contents than that in the JPGD. Czamanske and Mihalik (1972) reported that ilmenite crystallized under more oxidizing condition is enriched in Mn and depleted in Fe. Therefore, ilmenite of the KPGR accompanied by magnetite had crystallized under more oxidizing condition than that of the JPGD.

The whole-rock magnetic susceptibility of the granitic rocks was measured by Kappameter KT-5. The magnetic susceptibility of the KSGR ranges from 33 to 144 in 10^{-6} emu/g, which is higher than that of the JPGD (9~12). In the KSGR, the values of the KGPH, KPGR and KBGR are 33 to 80, 108 to 114 and 90 to 144 in 10^{-6} emu/g, respectively. Ishihara (1977) suggested the boundary value of the whole-rock magnetic susceptibility between magnetite-series and ilmenite-series granitoids is about 100 in 10^{-6} emu/g. However, the reported boundary values in some granitic masses are generally lower than the suggested one. For example, the boundary value for the Inje-Hongcheon granitic mass is 35 (Jwa, 1990) and that for the Tokuwa batholith is 45 in 10^{-6} emu/g (Shimizu, 1986). The higher magnetic susceptibility values represent that the granitic rocks belongs to the magnetite-series granitoids and emplaced in more oxidizing environment. Considering the boundary value of 35~45 in 10^{-6} emu/g, the KSGR generally belongs to the magnetite-series granitoid, whereas the JPGD to ilmenite-series. Thus the KSGR magma was solidified under the more oxidation environment than the JPGD magma. The whole-rock magnetic susceptibility data corroborate the result from the chemistry of biotite and ilmenite.

CONCLUSIONS

The studies on petrology and mineralogy of the granitic rocks in Poeun-Sogrisan area lead to the following conclusions.

1) The granitic rocks in study area are composed of Jurassic Poeun granodiorite and Cretaceous Sogrisan granitic rocks. The latter can be divided into coarse-grained biotite granite, porphyritic biotite granite and granite porphyry.

2) From the petrographical observations, it can be said that the Sogrisan granitic rocks, compared with the Poeun granodiorite, had been formed

from shallower-level emplaced and more rapidly crystallized granitic magma.

3) The F, Cl contents and the Fe/(Fe+Mg) ratios of biotite and muscovite in the Sogrisan granitic rocks are higher than those in the Poeun granodiorite. The An contents of plagioclase in the Poeun granodiorite are higher than in the Sogrisan granitic rocks. Alkali feldspar occurs as microcline in the Poeun granodiorite and as perthitic orthoclase in the Sogrisan granitic rocks. Ilmenite in the Sogrisan granitic rocks is more enriched in Mn and depleted in Fe than that in the Poeun granodiorite.

4) The Sogrisan granitic rocks had been solidified under more oxidation environment than the Poeun granodiorite, judging from the chemical compositions of minerals and the whole-rock magnetic susceptibility measurements.

ACKNOWLEDGMENTS

We wish to thank to Prof. M. Cho of Seoul National University and Prof. Y. J. Kim of Chonnam National University for their critical reviews of this manuscript. We are also grateful to Prof. H. T. Chon of Seoul Nat. Univ. for help using a Kappameter. This study was partly supported by the KOSEF 941-0400-007-1 and Ministry of Education BSRI-94-5404 (to Yong-Joo Jwa).

REFERENCES

Cho, D.L. and Kwon, S.T., 1994, Hornblende geobarometry of the Mesozoic granitoids in South Korea and the evolution of crustal thickness. J. Geol. Soc. Korea, 30, 41-61. (in Korean)

Cluzel, D., Cadet, J. P. and Lapierre, H., 1990, Geodynamics of the Ogcheon belt (South Korea). Tectonophysics, 183, 41-56.

Czamanske, G.K. and Mihalik, P., 1972, Oxidation during magmatic differentiation, Finnmarka complex, Oslo area, Norway: Part 1, The opaque oxides. J. Petrol., 13, 493-509.

Czamanske, G. K., Ishihara, S. and Atkin, S. A., 1981, Chemistry of rock-forming minerals of the Cretaceous-Paleocene batholith in Southwestern Japan and implication for magma genesis. J. Geophys. Res., 86, 10431-10469.

Hibbard, M.J., 1979, Myrmekite as a marker between preaqueous and postaqueous phase saturation in granitic systems. Geol. Soc. Am. Bull., 90, 1047-1062.

Iiyama, J.T. and Fonteilles, M., 1981, Mesozoic granitic rocks of southern Korea reviewed from major constituents and petrography. Mining Geol., 31, 281-295.

Ishihara, S., 1977, The magnatite-series and ilmenite-series granitic rocks. Mining Geol., 27, 293-305.

Jin, M.S., Kim, S.J., Shin. S.C., Choo, S.H. and Chi, S. J., 1992, Thermal history of the Jecheon granite pluton in the Ogcheon Fold Belt, South Korea. J. Petr. Soc. Korea, 1, 49-57.

Jwa, Y.J., 1990, Petrography and major element geochemistry of the granitic rocks in the Inje-Hongcheon district, South Korea. J. Min. Pet. Econ. Geol., 85, 98-112.

Kim, H.S., 1971, Metamorphic facies and regional metamorphism of Ogcheon metamorphic belt. J. Geol. Soc. Korea, 7, 221-256.

Kim, K.H. and Shin, Y.S., 1990, Petrochemistry of the granitic rocks in the Chungju, Wolaksan and Jecheon granite batholiths. J. Korean Inst. Mining Geol., 23, 245-259.

Kim, O.J., 1971, Study on the intrusion epochs of younger granites and thier bearing to orogenesis in South Korea. J. Korean Inst. Mining Geol., 4, 1-9.

Konings, R.J.M., Boland, J.N., Vriend, S.P. and Jansen, B.H., 1988, Chemistry of biotites and muscovites in the Abas granite, northern Portgal. Am. Mineral., 73, 754-765.

Lee, D.S., 1971, Study on the igneous activity in the middle Ogcheon geosynclinal zone, Korea. J. Geol. Soc. Korea, 7, 153-216.

Lee, D.S. and Park, J.S., 1981, A petrological study on the southwestern contact zone. J. Korean Inst. Mining Geol., 14, 55-76.

Lee, J.I., 1991, Petrology, mineralogy and isotopic study of the shallow-depth emplaced granitic rocks, southern part of the Kyoungsang Basin, Korea - Origin of micrographic granite. unpub. PhD thesis, Univ. of Tokyo, 197pp.

Lee, J.I. and Lee, M.S., 1991, Mineralogy and petrology on the granitic rocks in the Youngju Area, Kyoungsang Buk-Do, Korea. J. Geol. Soc. Korea, 27, 626-641.

Monier, G., Mergoil-Daniel, J. and Labernardiere, H., 1984, Generations successives de muscovite et feldspaths potassiques dans les leucogranite du massif de Millevaches (Massif Cetral Francais).

Bull. Mineral., 107, 55-68.

Nakamura, Y. and Kushiro, I., 1970, Compositional relations of coexisting orthopyroxene, pigeonite and augite in a tholeiitic andesite from Hakone volcano. Contrib. Mineral. Petrol., 26, 265-275.

Otoh, S., Jwa, Y.J. and Lee, M.S., 1990, Mesozoic ductile shear deformation in East Asia : Examples from South Korea. J. Geol. Geograph., 99, 388-390.

Powell, M. and Powell, R., 1977, Plagioclase-alkali feldspar geothermometry revisited. Mineral. Mag., 41, 253-256.

Shelly, D., 1964, On myrmekite. Am. Mineral., 49, 41-52.

Shibata, K., Park, N.Y., Uchiumi, S. and Ishihara, S., 1983, K-Ar ages of the Jecheon granite complex and related molybdenite deposits in South Korea. Mining Geol., 33, 193-197.

Shimizu, M., 1986, The Tokuwa batholith, Central Japan-An example of occurrence of ilmenite-series and magnetite-series granitoids in a batholith. The University Museum, Univ. of Tokyo, Bull., 28, 146

Simpson, C. and Wintsch, R.P., 1989, Evidence for deformation-induced K-feldspar replacement by myrmekite. J. metamorphic Geol., 7, 261-275.

Tsusue, A., Mizuta, T. and Hashimoto, K., 1984, Granitic rocks in Northern Kyushu. Mining Geol., 34, 385-399.

Tuttle, O. F. and Bowen, N. L., 1958, Origin of granite in the light of experimental studies in the system $NaAlSi_3O_8$-$KAlSi_3O_8$-SiO_2-H_2O. Geol. Soc. Am. Mem, 74, 153p.

Webster, J. D. and Holloway, J. R., 1990, Partitioning of F and Cl between magmatic hydrothermal fluids and highly evolved granitic magmas. Geol. Soc. Am. Spe. Paper, 246, 21-34.

Wones, D.R. and Eugster, H.P., 1965, Stability of biotite : experiment, theory and applications. Am. Mineral., 50, 1228-1272.

Yun, H.S. and Kim, S.E., 1990, Petrology and petrochemistry of the Cretaceous granites in the southern Munkyeong area. J. Korean Inst. Mining Geol., 23, 343-352.

(책임편집 : 김용준)

보은-속리산 지역의 화강암류에 대한 암석기재 및 광물화학

조원식* · 좌용주** · 이종익*** · 이민성*

*서울대학교 사범대학 지구과학과,

**경상대학교 자연과학대학 지질학과,

*** 한국해양연구소 극지연구센터

요 약 : 보은-속리산 지역의 화강암류는 쥬라기 보은 화강섬록암과 백악기 속리산 화강암류로 구성된다. 속리산 화강암류는 다시 세 가지의 암상, 즉 조립질 흑운모 화강암, 반상 흑운모 화강암 및 화강반암으로 세분된다. 암석에 대한 기재적인 관찰로부터, 속리산 화강암류는 보은 화강섬록암에 비해 천소에 관입하고 보다 빠르게 고결된 화강암질 마그마로부터 생성되었슴을 알 수 있다. 광물화학에서는 흑운모와 백운모의 F, Cl 함량과 Fe/(FeMg) 비가 보은 화강섬록암에 비해 속리산 화강암류에서 높게 나타나며, 사장석의 아노르사이트 함량은 보은 화강섬록암에서 높게 나타난다. 티탄철석의 경우 속리산 화강암류가 보은 화강섬록암보다 Mn이 풍부하고 Fe가 결핍된 경향을 보인다. 전암 대자율의 측정 결과는 속리산 화강암류가 $33\sim144\times10^{-6}$ emu/g로 보은 화강섬록암의 $9\sim12\times10^{-6}$ emu/g보다 높게 나타났으며, 이로부터 속리산 화강암류가 주로 자철석계열의 화강암류에, 보은 화강섬록암이 티탄철석계열의 화강암류에 속함을 알 수 있다. 전암 대자율의 결과와 흑운모 및 티탄철석의 화학조성 등은 속리산 화강암류가 보은 화강섬록암에 비해 보다 산화적인 환경에서 고결되었슴을 지시한다.

핵심어 : 보은 화강섬록암, 속리산 화강암류, 암석기재, 광물화학, 전암 대자율